A Study of Reynolds Number Effects and Drag-Reduction Concepts on a Generic Tractor-Trailer

Bruce L. Storms*
AerospaceComputing, Inc., Moffett Field, CA, 95223

and

Dale R. Satran†, James T. Heineck‡, Stephen M. Walker §
NASA Ames Research Center, Moffett Field, CA, 95223

The 1/8-scale Generic Conventional Model (GCM) was studied experimentally in the NASA-Ames 12-Foot Pressure Wind Tunnel. The GCM is representative of a Class-8 tractor-trailer with the engine in front of the cab. The investigation was conducted at a Mach number of 0.15 over a Reynolds number range from 500,000 to 6 million (equivalent to full scale at 75 mph). The experimental measurements included total and component forces and moments as well as 3-D particle image velocimetry (PIV). The results indicated minimal Reynolds number effects for most of the configurations investigated. Three configurations (side and roof extenders, trailer belly box, and base flaps) significantly reduced the drag of the vehicle. The addition of side and roof extenders to the back of the cab had a minimal effect at low yaw angles while significantly reducing the drag at higher yaw angles by up to 35%. The extenders yielded a wind-averaged drag reduction of 27% relative to the baseline without extenders. The trailer belly box with reduced ground clearance and covered wheels provided an additional drag reduction of 11.8% relative to the extender configuration. The addition of base flaps to the end of the trailer provided 19.4% drag reduction compared to the extender-only case.

Nomenclature

A	=	tractor-trailer frontal area = w*h
C_D	=	body-axis drag coefficient = D / q*A
D	=	body-axis drag
g	=	tractor-trailer gap
h	=	trailer height
q	=	test-section dynamic pressure = $^1/_2\ \rho U^2$
Re	=	Reynolds number = U*w / ν
A	=	tractor-trailer frontal area = w*h
U	=	free-stream velocity
w	=	trailer width
ν	=	kinematic viscosity
ρ	=	air density
ψ	=	yaw angle (positive nose right)

* Senior Research Engineer, Systems Analysis Branch, M/S 260-1, NASA Ames Res Ctr, Moffett Field, CA, 94035.
† Aerospace Engineer, Systems Analysis Branch, M/S 260-1, NASA Ames Res Ctr, Moffett Field, CA, 94035.
‡ Photographic Technologist, Systems Analysis Branch, M/S 260-1, NASA Ames Res Ctr, Moffett Field, CA,94035.
§ Research Scientist, Systems Analysis Branch, M/S 260-1, NASA Ames Res Ctr, Moffett Field, CA, 94035.

I. Introduction

FOR a typical heavy vehicle at a highway speed of 70 mph, the energy required to overcome aerodynamic drag is about 65% of the total expenditure (which also includes rolling friction, transmission losses, and accessories). By altering the vehicle shape, it has been estimated that modern truck drag coefficients may be reduced by up to 50% resulting in an annual national fuel savings of three billion gallons[1]. This large potential savings coupled with increasing fuel costs have spurred renewed interest in heavy-vehicle aerodynamics.

Previously, a significant number of experimental studies of heavy-truck geometries were conducted in the 1970's and 1980's[2]. The resulting first-generation drag-reduction technology currently in use includes cab shaping, cab-mounted deflectors, trailer front-end fairings, cab side extenders, and body front-edge rounding. The cab deflectors and side extenders accounted for the majority of the wind-averaged drag reduction reducing the pre-1980 drag level by about 25%. Other drag-reduction technologies that are not widely used include tractor-trailer gap seals, trailer side skirts, and rear boat-tailing. Each of these technologies produce a reduction of the wind-averaged drag coefficient between 0.03 and 0.10 which is about one-half the benefit of the first-generation technologies. However, the benefits of these devices are additive and the resulting net reduction is relatively large. The gap seal is a panel near the centerline of the truck that closes the tractor-trailer gap to lateral flow. Experimental measurements suggest that the use of the gap seal could replace the side extenders, thereby reducing the cost of a typical tractor aero package. Similarly, trailer side skirts reduced drag by blocking cross flow under the trailer and may also reduce spray as an added benefit. Lastly, the most practical boat-tailing device consisted of straight panels attached to the rear of the trailer side and roof edges and inclined towards the rear of the trailer. Results from 1:10-scale wind tunnel testing at a Reynolds number of 1.25 million yielded an optimum configuration with an angle of 15 degrees and a full-scale panel length of 20 inches.

Aerodynamic boat-tailing was also investigated on a full-scale tractor/trailer configuration in the 80- by 120-Foot Wind Tunnel at NASA Ames Research Center in 1988[3]. In this study, the boattail plates consisted of four panels that were mounted perpendicular to the aft-facing trailer door. The plates were inset from the edges of the trailer on three sides and mounted flush with the trailer edge on the bottom. This passive device traps recirculating flow between the plates and the rear corners of the trailer. As a result, the flow separating from the rear of the trailer is turned inward slightly. This yields an increase in the base pressure and a reduction in the overall drag. The optimum boattail plate configuration reduced the overall drag by about 10% at zero yaw angle. Relative to the baseline configuration (without plates), measurements indicated that the base pressure between the boattail plates was significantly increased while the pressure between the plates and the edge of the trailer was reduced.

More recently, a series of experimental and computational studies have been funded by the Department of Energy's Office of Heavy Vehicle Technologies. With the goal of CFD validation, the experimental efforts have focused on simplified geometries at 1:8-scale and below. Early experiments[4-6] focused on the simplified geometry of the Ground Transportation System (GTS) model representative of a class-8 tractor-trailer with a cab-over-engine design. A 1:8-scale GTS model with no tractor-trailer gap and no wheels was first studied with the addition of several ogival boattails and slants to the base of the trailer[4]. The largest overall drag reduction of 10% was obtained by an 8-ft ogive configuration (full scale). The addition of boattail plates to the same model resulted in a 19% drag reduction and PIV measurements behind the trailer document a significant reduction in the wake size due to the flow turning provided by the plates[5]. Variation of the tractor-trailer gap on a 1:15-scale model at zero yaw revealed relatively constant drag on the tractor while the trailer drag increases by a factor of three as the gap increases from zero to $1.55*\sqrt{A}$ (Ref. 6). Reynolds-averaged Navier-Stokes computations of this geometry[7] include both grid-size and turbulence-model studies.

In addition to the passive devices mentioned above, several pneumatic drag-reduction concepts have also been studied. One study[8] investigated the use of blowing slots on the leading and trailing edges of the trailer. For a simplified 1:15-scale cab-over geometry with an oversized tractor-trailer gap (84 inches full scale), the drag reduction was over 50% with 1-psig blowing pressure (mass-flow coefficient = 0.13) and considerably higher with additional blowing. Other forces and moments were generated by blowing selected slots and slot combinations. Another study[9] investigated the effect of base bleed on a simplified bluff-body shape representative of a square-back passenger car. By injecting low-velocity air into the base region through a porous surface, drag reduction of 7.5% was achieved with a mass-flow coefficient of 0.3 and a surface porosity of 33%. Surprisingly, zero flow rate produced a drag reduction of approximately half this value (3.7%) indicating the passive effect of a porous base. The drag reduction was also found to increase with increasing base-bleed area.

The Generic Conventional Model of the current study was previously investigated at a Reynolds number of 1.1 million in the NASA-Army 7- by 10-Ft Wind Tunnel[10]. The results include forces and moments, surface pressures, and 3-D particle-image velocimetry. Measurements of two tractor-trailer gaps (40 and 80 inches full scale) indicated significantly greater drag for the larger gap at low yaw angles (between ±4 deg) and reduced drag at higher angles. Several drag-reduction concepts were investigated including tractor side extenders, boattail plates, and a trailer belly box. Comparisons of PIV data were presented in the tractor-trailer gap with and without side extenders and in the trailer wake with and without boattail plates[11].

The goal of the present study was to investigate Reynolds-number effects and provide quality experimental data on a simplified tractor-trailer geometry for CFD validation. By varying the total pressure of the wind tunnel, it was possible to vary the Reynolds number from 500,000 to full-scale values over 6 million based on trailer width. In addition to the force, moment, and pressure measurements, off-body details were provided by 3-D particle image velocimetry. Measurements were made at various yaw angles to study the influence of crosswind and to calculate wind-averaged drag coefficients. Several drag-reduction concepts were studied in order to document their potential benefit as well as their Reynolds-number sensitivity.

II. Experimental Setup

The investigation was conducted in the 12-Foot Pressure Wind Tunnel located at NASA Ames Research Center. This facility can be pressurized from 0.25 to 6 atmospheres at Mach numbers from 0.1 to 0.5. The test section has a circular cross section 12 ft in diameter with four 4-ft wide flat surfaces centered about the horizontal and vertical centerlines. A ground plane was installed 21 inches above the tunnel floor providing a flat surface 10 ft wide and 18 ft long. Pressure taps were located on both the ground plane (2 rows of 64 taps) and the test-section walls (8 rows of 30 taps). A fairing was installed to isolate the model-support hardware from the air stream, and speed-correction probes were used to correct the facility speed due to the blockage of the ground plane and fairing. There was also an additional pitot-static probe installed on the upper left ceiling to measure the free-stream conditions in the test section. All of the data presented is referenced to the Mach number based on a wall tap at location 6.17 ft forward of the center of rotation at an azimuth of 60 deg from vertical (two o'clock looking downstream).

A photograph of the GCM baseline configuration installed in the wind-tunnel test section is shown in Fig. 1. This 1:8-scale model is representative of a generic class-8 tractor-trailer with the engine in front of the cab. Designed for CFD validation, the model includes a number of geometry simplifications in order to facilitate grid generation and avoid the associated flow complexities. In particular, no effort was made to duplicate the complex geometry of the undercarriage of either the tractor or trailer (both were approximated by flat surfaces). Similarly, the wheel wells of the tractor were not modeled and only the portion of the wheels below the tractor lower surface were included (Fig. 2). Also, the tractor geometry (designed by the Calmar Research Corp.) is a streamlined shape representative of a modern tractor design while omitting most small-scale surface details and flow-through components. The trailer measures 45 ft in length (full scale) with rounded front vertical edges (8-in full-scale radius). The tractor-trailer gap for this study was held constant at the full-scale equivalent of 40 inches. The GCM was attached to the model-support hardware with four vertical posts that were 1.75 inches in diameter. The four posts were non-metric with 0.030 inches of clearance as they passed through the trailer floor. The model was mounted with its wheels 0.15 inches above the ground plane and centered laterally in the tunnel. The center of rotation of the model was located 54.36 inches aft of the tractor front bumper. The model frontal area of 1.6623 ft^2 gives a solid blockage of 1.5%.

The overall model loads were measured with a six-component internal balance (4.0" Task balance Mark 2B) that was mounted inside the trailer. The manufacturer-specified accuracy of the internal balance in the axial (drag) direction was ± 1 lb, but repeat runs indicated the experimental uncertainty to be on the order of ±0.5 lb. The tractor was suspended from the trailer through a set of flexures and 2 load cells that measure the drag and yawing moment of the tractor alone. The specified accuracy of the load cells was ±0.45 lb. The model was instrumented with 200 pressure taps on the tractor and 276 taps on the trailer. There were also 12 unsteady pressure transducers mounted on the tractor rear surface, trailer front surface, and the trailer rear surface. A three-component particle image velocimetry (PIV) system was used to obtain horizontal-plane velocity measurements in the tractor-trailer gap. Details of the PIV system installation are presented in Ref. 12. Pressure measurements will be documented in a future report.

The model was yawed through a range of angles between ±14 degrees. Except where noted, all data were acquired at a Mach number of 0.15 which allowed for Reynolds number studies with no Mach-number effects. With the tunnel pressurized to six atmospheres, the Reynolds number was over 6 million based on the trailer width which is comparable to a full-scale truck driving at 75 mph. At one atmosphere, the Reynolds number was 1 million based on the trailer width which is comparable to a full-scale truck driving at 15 mph.

Various add-on drag-reduction devices were tested on the bases of both tractor and trailer as well as on the trailer under-carriage. In this report, results will be presented for tractor side and roof extenders, trailer boattail and base flaps, and trailer belly box and skirts. Details of each device will accompany the discussion of the associated results.

III. Results and Discussion

The results presented below detail the body-axis axial force (drag) coefficient for the tractor-trailer combination and its components. This drag coefficient represents the force along the axis of the vehicle in the direction of travel. The internal balance also provided lift, side force, and moment measurements which will not be discussed. With the objective of CFD validation, no wall corrections were applied to the data and all coefficients were calculated based on the static pressure at a known point in the test section (as detailed above). Without wall corrections, the computed drag coefficients will differ from those of the equivalent model in free air. However, the measured differences between configurations should be representative of the effects of the associated geometric modifications.

The drag data presented herein were acquired for increasing yaw angle unless otherwise noted. Using the variation of drag with yaw angle, wind-averaged drag coefficients were computed using the SAE Recommended Practice of Ref. 13. This practice assumes that the mean wind speed in the United States of 7 mph has an equal probability of approaching the vehicle from any direction. This mean wind speed and the vehicle velocity were used to calculate a weighted average of the drag coefficient at various yaw angles. The wind-averaged drag coefficients reported in this paper were computed for a highway speed of 55 mph.

A. Baseline Configuration

The baseline geometry for this study is representative of a modern tractor design with the standard aero package less the side or roof extenders. Yaw angle sweeps for increasing and decreasing angle revealed significant hysteresis in the resulting drag measurements (Fig. 3). Since the drag curve of a simplified geometry with no gap is relatively continuous[5], the discontinuities at high yaw angles are likely due to changes of the flow structures within the tractor-trailer gap. The effect of Reynolds number is most evident at the yaw angles greater than 8 deg where the peak drag and hysteresis are notably different. At lower yaw angles, however, the differences are relatively small and the hysteresis paths are nearly duplicated. For a mean crosswind of 7 mph ($-7.2 < \psi < 7.2$) as shown in Fig. 3, the wind-averaged drag coefficients at Reynolds numbers of 1 and 6 million (0.582 and 0.578, respectively) differed by less than 1%. A look at the component drag coefficients at Re = 6 million (Fig. 4) reveals discontinuities in the drag curve of the tractor and a more continuous curve for the trailer. The hypothesized change in flow structure in the tractor-trailer gap is likely responsible for both the discontinuities in the tractor drag curve and the associated drop-off in measured drag on the trailer.

A three-component PIV system was employed for velocity measurements in the tractor-trailer gap. The velocity vector maps (Figs. 5-7) are averages of 100 discrete measurements acquired at 2 Hz in intermittent bursts (due to computer limitations) over a period of three minutes. Although data were acquired at 1/4, 1/2, and 3/4 trailer heights, the results presented in this report are limited to the topmost location. In these figures, the direction and magnitude of the vectors indicate the in-plane velocities while the color map indicates the out-of-plane (vertical) velocity. The velocity vector maps for zero yaw (Fig. 5) reveal two counter-rotating recirculation regions in the gap and suggest minimal sensitivity to Reynolds number. The yaw angle of –10 deg (Fig. 6), however, is in the hysteresis region of the drag curves where there are significant differences between two Reynolds numbers. Both measurements were obtained for decreasing yaw angle that correspond to the upper curves as indicated in Figure 3. Similar to the zero-yaw case, the flowfield at Re = 5 million exhibits two recirculation regions, but they are strongly asymmetric and with much higher velocities. At Re = 1 million, only the tight recirculation on the windward (left) side is present and there are significantly greater crossflow and downward velocities compared to the higher Reynolds number. The corresponding drag coefficient for Re = 1 million is 2% higher than that for Re = 5 million. The lower measurement locations revealed similar flow structures to the topmost height, but with reduced Reynolds-number sensitivity.

The PIV data also provide insight into the drag-curve hysteresis. A look at two neighboring yaw angles near –10 deg reveal drastically different flowfields at one Reynolds number (Fig. 7). As indicated on the drag curves (Fig. 3), these two measurements correspond to yaw angles of –10 deg (decreasing) and –10.5 deg (increasing) at Re = 1 million. For the yaw angle of –10.5-deg, the windward recirculation region is absent and the velocities in the gap are significantly lower than the –10-deg case. It is hypothesized that lower gap velocities yield higher pressures on the back of the cab (less drag) and a smaller separation region on the leeward (right) side of the truck (not visible in PIV images). As a result, the drag of the –10.5-deg case is 28% lower than that of the –10-deg case.

B. Side and Roof Extenders

Similar to the components of a modern tractor aero package, side and roof extenders were attached to the rear of the tractor as shown in Figure 8. The extenders were 1/8-in thick (model scale) with four different lengths ranging from 30% to 60% of the tractor-trailer gap. For a length of 60% gap (as shown), the total drag coefficient as a function of yaw angle (Fig. 9) illustrates the dramatic effect of the extenders. At yaw angles less than 2 deg, the drag reduction is minimal while at higher angles the reduction increases dramatically to 35% at 10 deg. At a Reynolds number of 6 million, wind-averaged drag coefficient of 0.422 for the 0.6g extenders was 27% lower than that of the baseline without extenders. The low Reynolds-number measurements were marginally higher than those of the full-scale Reynolds number until about 10 deg yaw the curves cross and the low-Re drag drops off at the highest yaw angle of 14 deg. PIV data for this model with extenders were acquired previously in the NASA Ames 7- by 10-Ft Wind Tunnel at a Reynolds number of 1 million[11]. The results indicate a significant reduction in the gap cross flow due to the presence of the side and roof extenders.

The component drag curves with extenders at Re = 6 million (Fig. 10) reveal that the drag of the tractor is significantly reduced even at low yaw angles where the total drag curve indicated minimal effect. This is likely due to an increase in pressure on the base of the tractor afforded by the extenders. Conversely, the drag of the trailer is shown to increase at yaw angles between ±6 deg with the addition of the extenders, likely due to reduced velocities and increased pressure in the gap region.

The wind-averaged drag reduction provided by the extenders is plotted as a function of extender length in Figure 11. For the four extender lengths tested between 30% and 60% gap width, there is a consistent trend of increasing drag reduction with increasing extender length. More specifically, the drag reduction increases from 25% to 27% for an increase in extender length from 30% gap to 60% gap. Although greater extender lengths may be impractical from an operational standpoint, this data suggests that additional drag reduction may be obtained by completely blocking the gap crossflow. As demonstrated in Ref. 2, a centerline gap seal can be more effective than the side extenders of a standard tractor aero package.

To determine the effect of Reynolds number, the facility total pressure was varied while the Mach number was held constant. The change in wind-averaged drag coefficient with Reynolds number (Fig. 12) reveals differing sensitivities for the baseline and extender configurations. In this figure, the error bars on the baseline data points show the magnitude of experimental uncertainty due to both measurement resolution and repeatability. Error bars were of the same magnitude for the extender configuration, but were omitted from the figure for clarity. For the baseline, the drag coefficient is observed to increase by an average of 0.006 (1%) for Reynolds numbers less than 4 million. The extender configuration, however, does not indicate a significant increase until below 3 million with a dramatic increase, close to 0.03 (6.9%), at Re = 500,000. The drag curves for the extender configuration at several Reynolds numbers (Fig. 13) illustrate a significant increase in drag that increases with crossflow at Re = 500,000. This is likely due to flow variations in the vicinity of the trailer leading-edge curvature which is more sensitive to Reynolds number than sharp corners.

C. Aerodynamic Boattail Plates

Since the side and roof extenders are first-generation drag-reduction devices common to most modern tractor aero packages, the effect of the boattail plates (and all subsequent devices) will be measured relative to the extender configuration. Aerodynamic boat-tailing devices have several different variations, but boattail plates typically refer to panels mounted perpendicular to the trailer base and inset from the edges of the trailer. In this case, the same boattail plates that were studied on the simplified GTS model[5] were applied to the rear of the GCM trailer as shown in Figure 14. The plates extended 3.75 in from the end of the trailer and were inset from the sides and top of the trailer by 0.625 in. The bottom plate was mounted flush with the bottom of the trailer.

Relative to the side and roof extenders, the boattail plates significantly reduced the drag by a relatively constant margin between ±10 deg (Fig. 15). At Re = 6 million, the wind-averaged drag coefficient was 0.364 which is 13.7% less than the extenders-only configuration. Relative to the high Reynolds-number case, the drag curve for the boattail plates at Re = 1.1 million exhibited the same roll off at high yaw angles as that of the side extenders alone. The results were mixed at lower angles with the low-Re curve lower than the high-Re curve at negative yaw angles and higher at some positive yaw angles. These mixed results are evident in the resulting wind-averaged drag coefficients which differ by only 0.6%.

The component drag curves at Re = 6 million (Fig. 16) indicate that all drag reduction from the boattail plates is due to reduced drag on the trailer. This is to be expected since the boattail plates serve to increase the pressure on the trailer base with no effect on the flow around the tractor.

D. Trailer Base Flaps

Another method of aerodynamic boat-tailing is what will be referred to as base flaps. In this embodiment, the panels are attached to the edges of the trailer base and angled inward. In the current study, measurements were made for a base-flap length of 3.125 inches (25 inches full scale) at angles ranging from zero to 28 deg. The installation photo (Fig. 17) shows the base flaps with a 20-deg deflection mounted on the rear of the trailer. Note that the linkages connecting the flaps to the base were designed for easy angle change and are not representative of the full-scale hardware.

The effect of the base flaps on the total drag coefficient is presented in Figure 18 for a flap angle of 16 deg. Relative to the side and roof extenders alone, the addition of the base flaps provide significant drag reduction that marginally increases with yaw angle. The Reynolds-number sensitivity of the base flaps is minimal for most yaw angles between ±10 deg. As in the previous configurations, the drag for Re = 1.1 million rolls off at the higher yaw angles while the drag at full-scale Reynolds number continues to increase. The component drag curves (Fig. 19) illustrate that, similar to the boattail plates, the base flaps reduce the drag on the trailer with minimal effect on the tractor.

The effect of base-flap angle on wind-averaged drag reduction is presented in Figure 20. Different symbols are used to indicate the data from two separate wind-tunnel entries (four months apart) of the same model in the NASA Ames 12-Ft Pressure Wind Tunnel. The lower Reynolds number on the second entry was due to limitations of the coincident PIV measurements. Although there is an unexplained offset in the two curves (marginally larger than the experimental uncertainty), the trends indicate that the optimum base-flap angle is around 20 deg. The wind-averaged drag coefficient with 20-deg base flaps is 0.340 which is 19.4% less than the extender configuration and 6.6% less than the boattail-plate configuration. Previous small-scale experiments[2] at a Reynolds number of 1.25 million yielded an optimum base-flap configuration with an angle of 15 degrees and a full-scale panel length of 20 inches. The difference between these two experiments is likely due to the differences in the base-flap lengths since the Reynolds-number effects were observed to be minimal. However, the effect of Reynolds number might be more significant at higher flap angles where the flow reattachment on the base flaps is more sensitive.

E. Trailer Belly Box and Skirts

Several drag-reduction concepts were studied with the goal of reducing the lateral flow under the trailer. Similar to previous studies, trailer side skirts consisted of flat panels extending downward from the sides of the trailer between the end of the tractor bed and the front of the trailer wheels. The full-skirt configuration extended to the rear of the trailer covering the trailer wheels and also included lateral panels at the trailer base and behind the tractor bed. The trailer belly box (Fig. 21), so named because of its resemblance to the design of moving trailers, was identical to the full-skirt configuration with the addition of a horizontal surface at the bottom of the skirt to form a box on the undercarriage of the trailer. All of these configurations had a full-scale ground clearance of 11.8 inches.

The varying effect of the trailer belly box and skirts on the overall drag is presented in Figure 22 for Re = 6.3 million. Relative to the extender-only case, the trailer belly box was the most effective with a wind-averaged drag reduction of 11.8%. The side skirts were somewhat less effective with a drag reduction of 6.2% while the full-skirt configuration increased the wind-averaged drag by 3.8%. The increase in drag of the full-skirt configuration is likely due to the cavity flow that forms inside the skirt. The wind-averaged drag coefficients for these three cases were 0.372, 0.396, and 0.438, respectively. Due to time limitations, a Reynolds-number sensitivity study was not performed for these configurations. The component drag curves at Re = 6.3 million (Fig. 23) indicate that the addition of the belly box affects the drag of both the tractor and trailer. The trailer drag reduction is relatively small at low yaw angles and increases at higher angles. A significant portion of this drag reduction is likely due shielding of the trailer wheels to cross flow which increases with yaw angle. The drag reduction of the tractor is relatively constant at yaw angles greater than 4 deg and less than –4 deg while there is a slight drag bucket in between. The tractor drag reduction is the likely result of increased base pressure on the tractor cab due to reduced crossflow between in the tractor-trailer gap.

IV. Summary

Experimental measurements were obtained of a 1:8-scale generic class-8 tractor-trailer model in the NASA Ames 12-Ft Pressure Wind Tunnel. The total pressure of the wind tunnel was varied at a constant Mach number of 0.15 to obtain Reynolds numbers based on trailer width between 500,000 and 6 million. Overall forces and moments were measured by an internal balance while the tractor drag was measured by load cells. A 3-D particle-image velocimetry system was used to obtain velocity measurements in the tractor-trailer gap for the baseline configuration without side and roof extenders. Several drag-reduction concepts were tested including tractor side and roof extenders, trailer aerodynamic boat-tailing, and trailer undercarriage flow barriers.

For all configurations, the effect of Reynolds number was most evident at high yaw angles ($\psi > 8$deg and $\psi < -8$deg) where there was a significant reduction in drag at lower Reynolds numbers. However, this difference did not significantly affect the computation of the wind-averaged drag coefficients at 55 mph which uses data at lower yaw angles. As a result, the variation of Reynolds number for the baseline revealed an increase in the wind-averaged drag on the order of 1% for Re ≤ 3 million. The Reynolds-number sensitivity for side and roof extenders was more dramatic with an increase in wind-averaged drag of over 7% for Re = 500,000. Limited data for the boat-tail devices suggest that the Reynolds-number sensitivity is similar to that of the baseline. No Reynolds-number study was performed for the undercarriage flow barriers.

The PIV measurements in the tractor-trailer gap document significant crossflow velocities and recirculation regions at yaw angles near 10 deg. Baseline measurements with reduced drag exhibited significantly reduced crossflow and less coherent recirculation regions. Since the tractor side and roof extenders function to reduce the gap crossflow and increase the tractor back pressure, the addition of the extenders to the baseline reduced the measured drag at all yaw angles. This reduction was dramatic at high yaw angles (35% at 10 deg) and minimal at low angles (2% at 0 deg). Of the four extender lengths tested (0.3 – 0.6 gap), the longest extenders were most effective yielding a 27% reduction in the wind-averaged drag coefficient. Since extenders are a standard component of a modern tractor aero package, the effectiveness of the remaining drag-reduction concepts were measured relative to this extender configuration (Table 1). Note that no wall corrections were applied to the experimental measurements in order to facilitate comparison with CFD simulations. However, the influence of the tunnel walls was minimized by calculating the tunnel speed based on the static pressure at a location adjacent to the model.

Table 1: Effect of drag-reduction concepts on wind-averaged drag.

Configuration	ΔC_D, 55 mph	% difference
No Extenders	+0.156	+37.0
Extenders	0	0
Boattail plates	−0.058	-13.7
Base flaps (20 deg)	−0.092	-19.4
Trailer belly box	−0.050	-11.8
Trailer side skirts	−0.026	-6.2
Trailer full skirt	+0.016	+3.8

Of the boat-tailing concepts (boattail plates and base flaps), the base flaps were found to be most effective. Base-flap angles from zero to 28 deg were studied resulting in an optimum angle of 20 deg. This result is higher than a previous low Reynolds-number study and may suggest some Reynolds-number sensitivity of the base-flap angle. The trailer belly box was the most effective trailer-undercarriage concept with almost double the drag reduction of simple side skirts. The belly box and full skirt configurations were identical except for the lower-surface enclosure of the belly box. The drag of the full-skirt configuration, however, was increased while that of the belly-box configuration was significantly reduced. This result stresses the importance of eliminating cavity flows to minimize drag.

This report presents only a fraction of the data generated by the experimental investigation of the GCM in the 12-Ft Pressure Wind Tunnel. A future archival test report will include additional force and moment data and PIV measurements as well as steady and unsteady model surface pressures.

Acknowledgments

This work was funded by the Department of Energy, Office of Heavy Vehicle Technology, under the direction of Dr. Sid Diamond. Significant input into the planning for this experiment came from the members of the Working Group on Heavy Vehicle Aerodynamic Drag headed by Rose McCallen of Lawrence Livermore National Laboratory.

References

[1]McCallen R., Flowers, D., Dunn, T., Owens, J., Leonard, A., Brady, M., Brownad, F., Hammache, M., Salari, K., Rutledge, W., Ross, J., Storms, B., Heineck, J.T., Driver, D., Bell, J., Zilliac, G., Walker, S., "Aerodynamic Drag of Heavy Vehicles (Class 7-8): Simulation and Benchmarking," 2000-01-2209, SAE Gov/Industry Meeting, Washington, D.C., June 19-21, 2000.

[2]Cooper, K. R., "Truck Aerodynamics Reborn – Lessons from the Past," SAE Paper 2003-01-3376, November 2003

[3]Lanser, J. M., Ross, J. C., and Kaufman, A. E., "Aerodynamic Performance of a Drag Reduction Device on a Full-Scale Tractor/Trailer," SAE Paper 912125, September 1991.

[4]Croll, R. H., Gutierrez, W. T., Hassan, B., Suazo, J. E., and Riggins, A. J., "Experimental Investigation of the Ground Transportation Systems (GTS) Project for Heavy Vehicle Drag Reduction," SAE Paper 960907, February 1996.

[5]Storms, B.L., Ross, J.C., Heineck, J.T., Walker, S.M., Driver, D.M. and Zilliac, G.G., "An Experimental Study of the Ground Transportation System (GTS) Model in the NASA Ames 7- by 10-Foot Wind Tunnel." NASA/TM-2001-209621, February 2001.

[6]Hammache, M., Michaelian, M., and Browand, F. "Aerodynamic Forces on Truck Models, Including Two Trucks in Tandem," SAE Paper 2002-01-0530, March 2002.

[7]Salari, K. and McWherter-Payne, M., "Computational Flow Modeling of a Simplified Integrated Tractor-Trailer Geometry," Sandia National Lab., Rept. SAND2003-3383, Albuquerque, NM, Sept. 2003.

[8]Englar, R. J., "Advanced Aerodynamic Devices to Improve the Performance, Economics, Handling and Safety of Heavy Vehicles," SAE Paper 2001-01-2072, May 2001.

[9]Howell, J., Sheppard, A., and Blakemore, A., "Aerodynamic Drag Reduction for a Simple Bluff Body Using Base Bleed," SAE Paper 2003-01-0995, March 2003.

[10]Satran, D., "Generic Conventional Model (GCM) Truck Test in 7x10 and 12-Ft," April 2002 Working Group Meeting on Heavy Vehicle Aerodynamic Drag, Lawrence Livermore National Laboratory, Livermore, CA, 2002 (unpublished).

[11]Heineck, J. T., Walker, S. M., and Satran, D., "The Measurement of Wake and Gap Flows of the Generic Conventional Truck Model (GCM) using Three-Component PIV," The Aerodynamics of Heavy Vehicles: Trucks, Buses and Trains, Monterey-Pacific Grove, CA, Dec. 2002

[12]Heineck, J. T., Walker, S. M., and Yaste, D. M., "The Development of a 3C-PIV System for the 12-Foot Pressure Tunnel at NASA Ames Research Center," *International Congress on Instrumentation of Aerospace Simulation Facilities*, Goettingen, Germany , August, 2003.

[13]"SAE Wind Tunnel Test Procedure for Trucks and Buses," SAE J1252 JUL81, SAE Recommended Practice, July 1981.

Figure 1: The Generic Conventional Model installed on the ground plane in the 12-Ft Pressure Wind Tunnel.

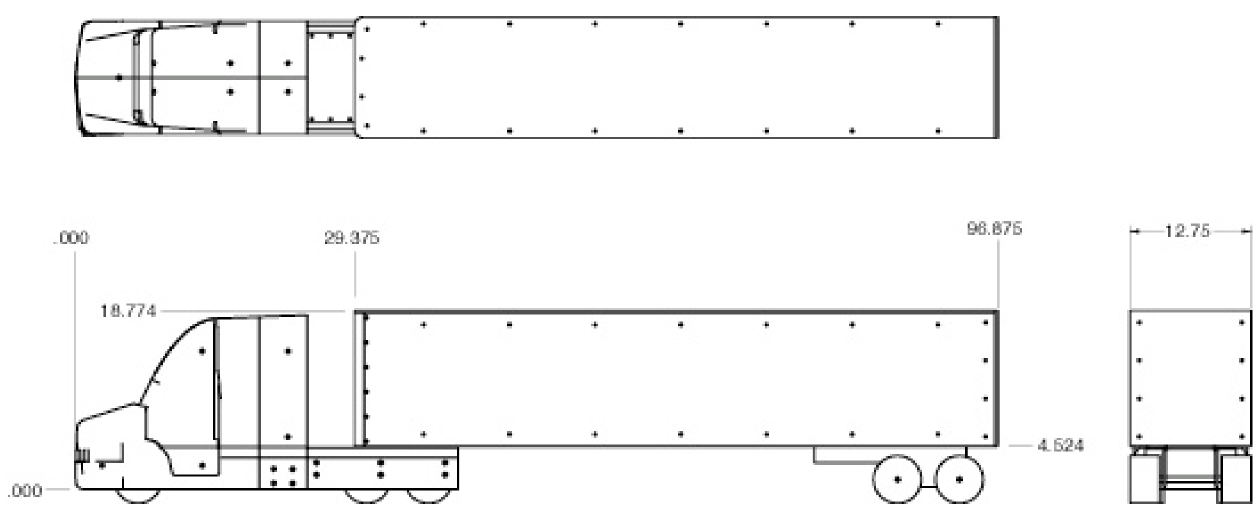

Figure 2: Three-view drawing of Generic Conventional Model.

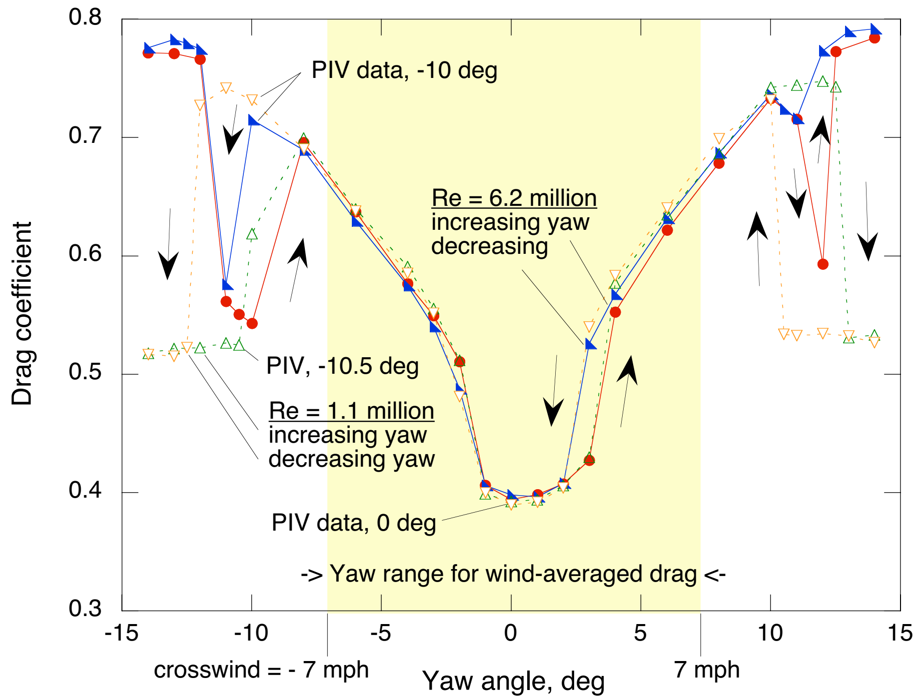

Figure 3: Baseline hysteresis of drag coefficient for two Reynolds numbers. Crosswind limits based on 55 mph road speed.

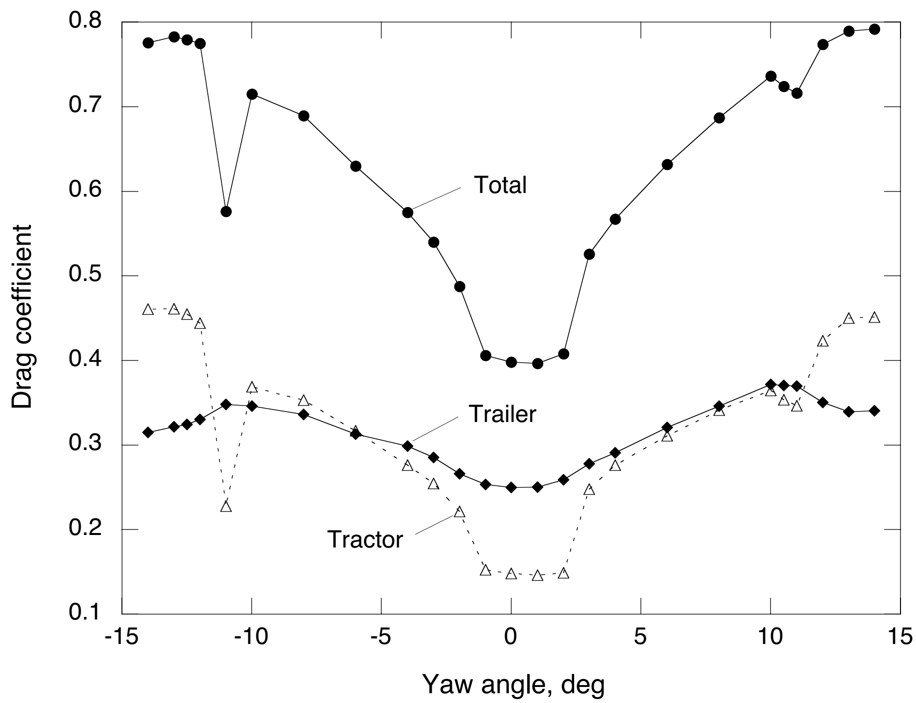

Figure 4: Component drag curves for baseline configuration at Re = 6 million.

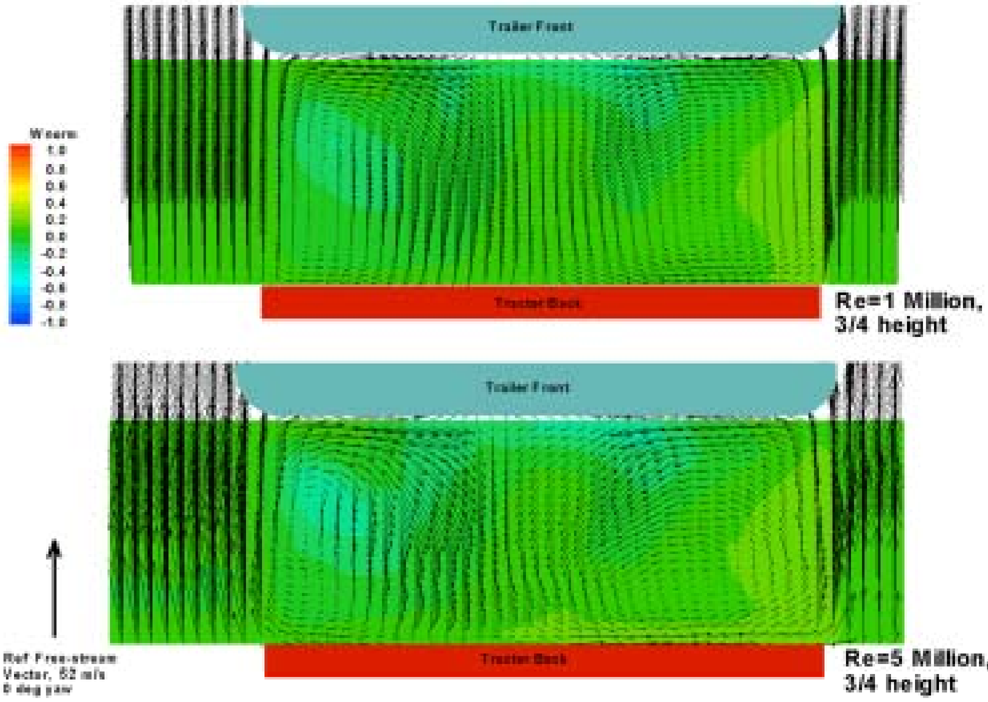

Figure 5: Particle Image Velocimetry measurements in the tractor-trailer gap at yaw = 0 deg. Top view of horizontal PIV data plane at 0.75h.

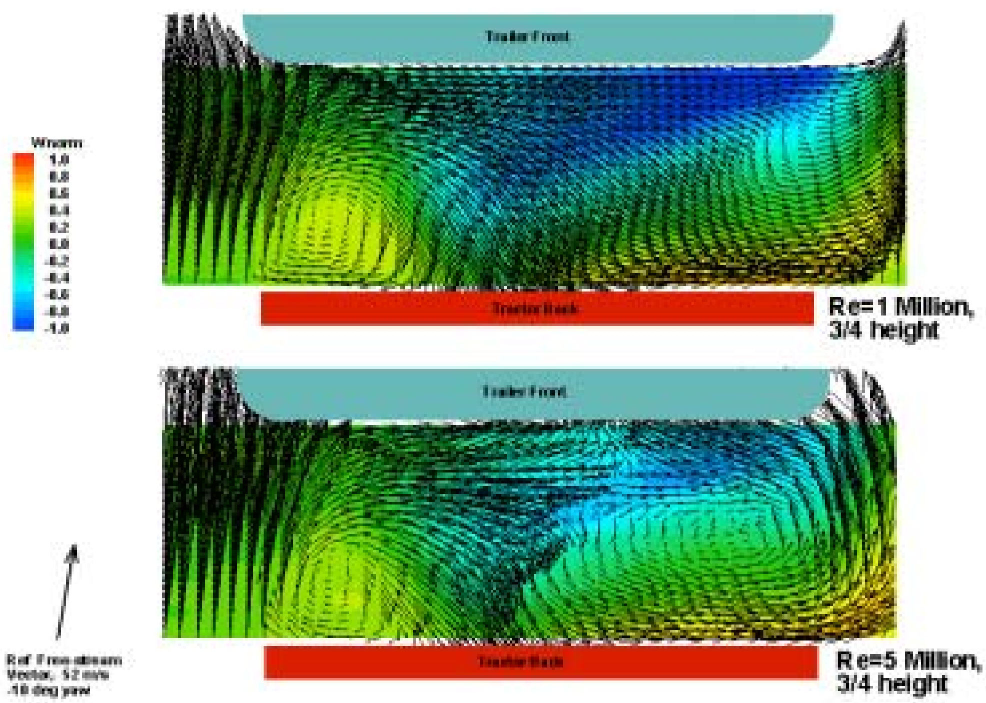

Figure 6: Particle Image Velocimetry measurements in the tractor-trailer gap at yaw = -10 deg

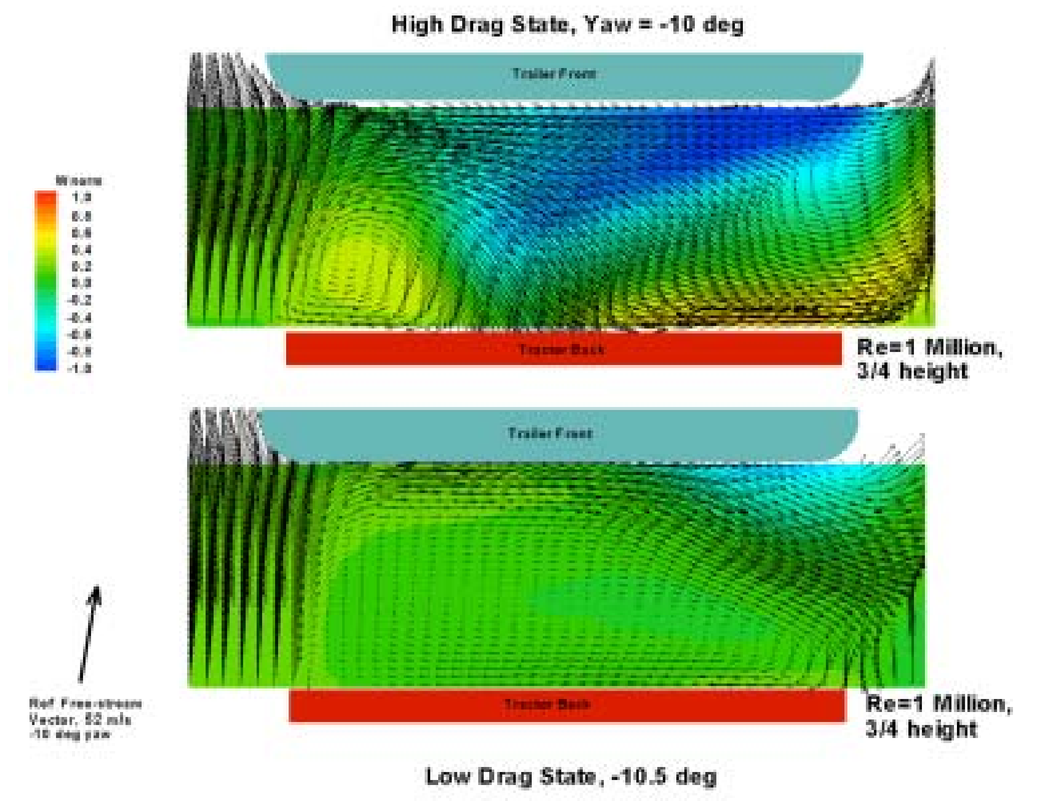

Figure 7: PIV measurements in the tractor-trailer gap for high- and low-drag states near -10 deg. Top view of horizontal PIV data plane at 0.75h.

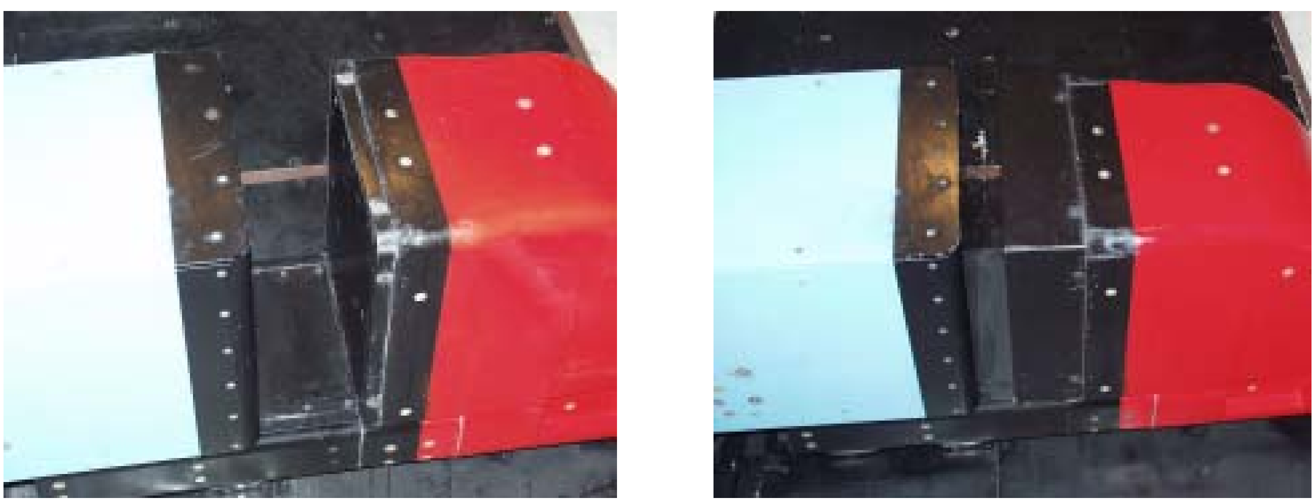

a) Baseline Configuration **b) Side and Roof Extenders (0.6g)**

Figure 8: Close-up of tractor-trailer gap with and without side and roof extenders.

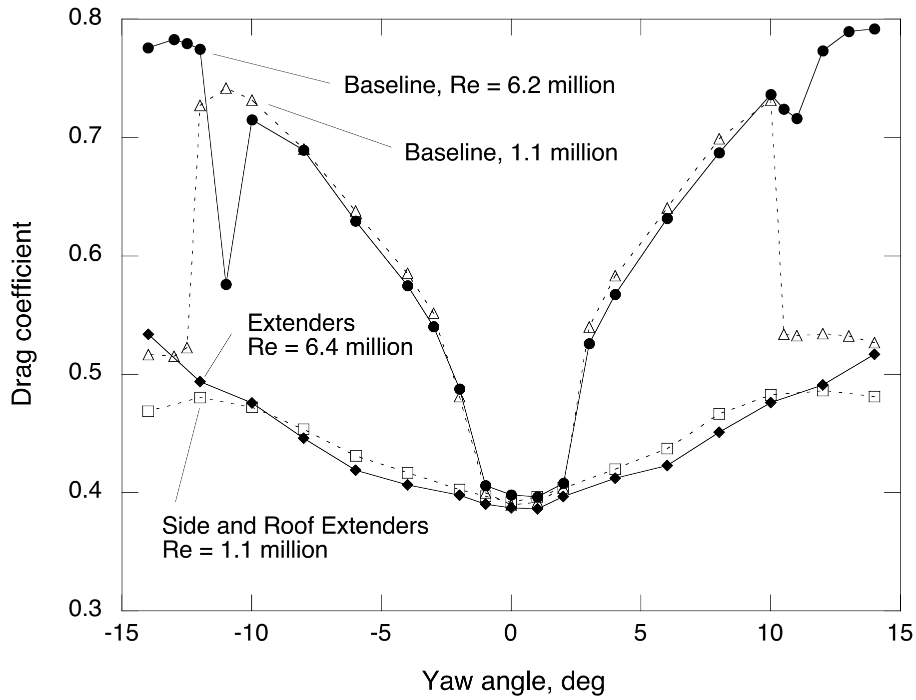

Figure 9: Effect of tractor side and roof extenders (0.6g) on total drag coefficient.

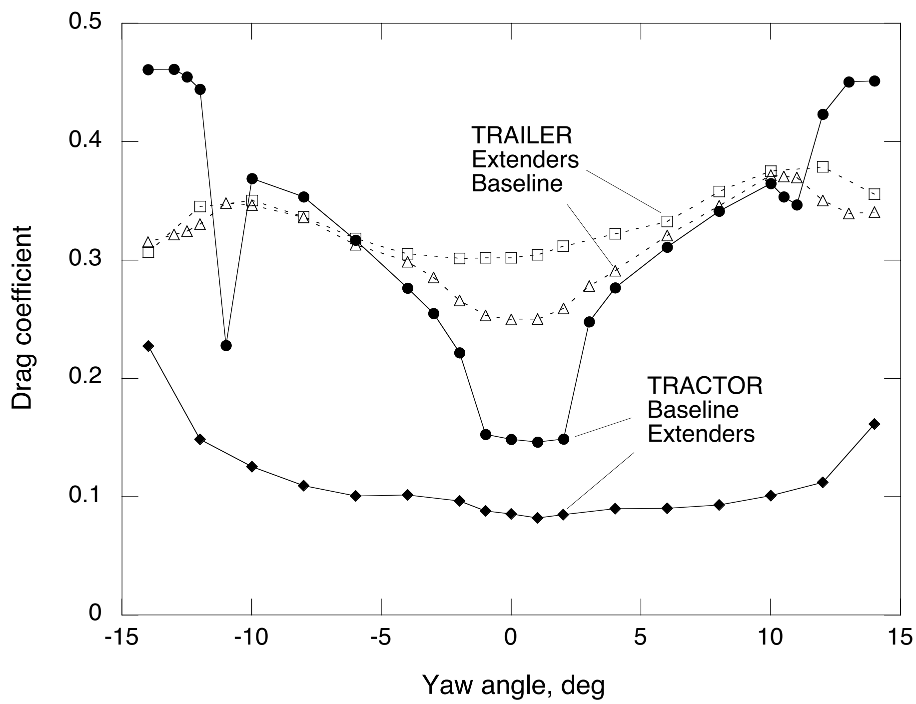

Figure 10: Effect of tractor side and roof extenders on component drag curves at Re = 6 million.

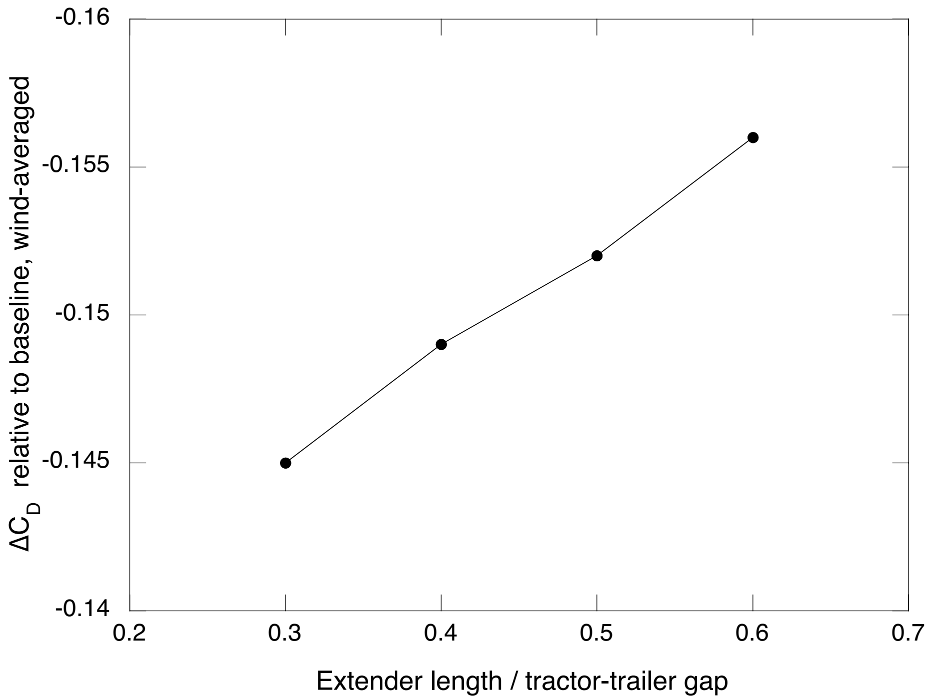

Figure 11: Wind-averaged drag reduction due to side and roof extenders at Re = 6 million.

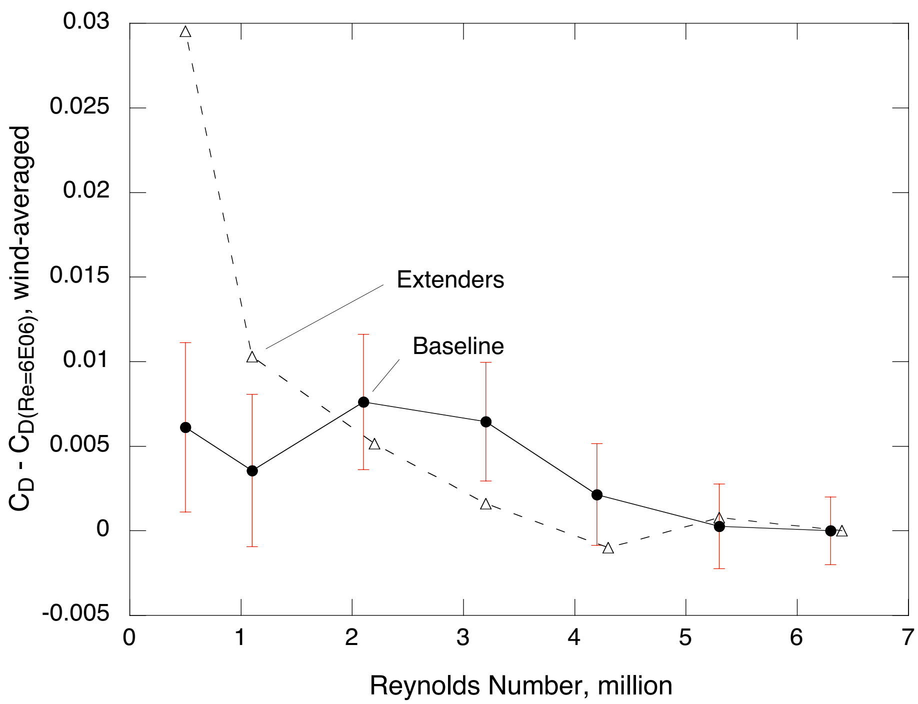

Figure 12: Reynolds-number sensitivity of wind-averaged drag for baseline and extender configurations.

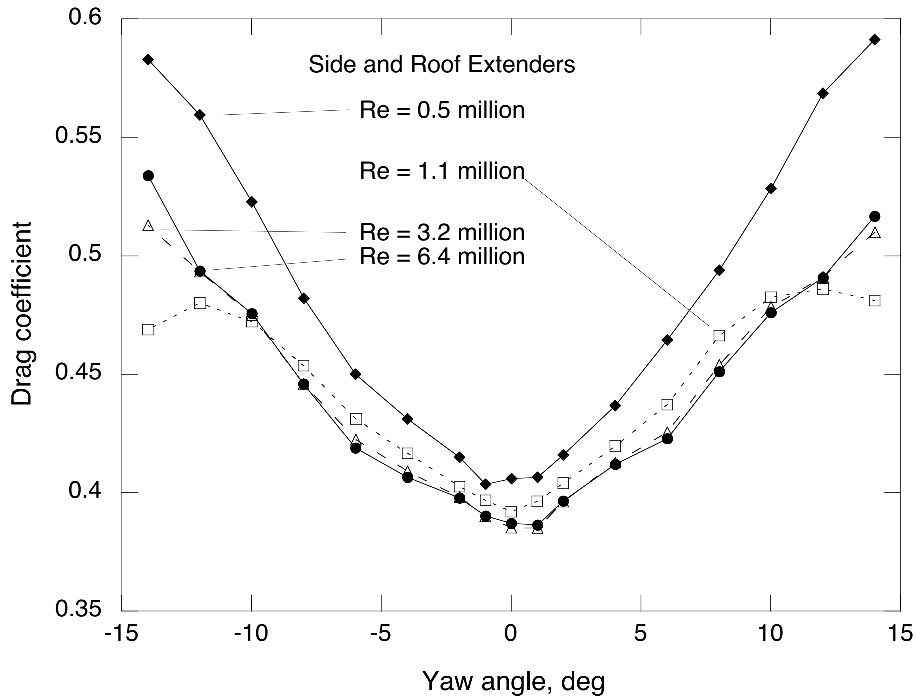

Figure 13: Reynolds-number sensitivity of side and roof extenders on drag curves.

Figure 14: Aerodynamic boattail plates installed on the base of the trailer.

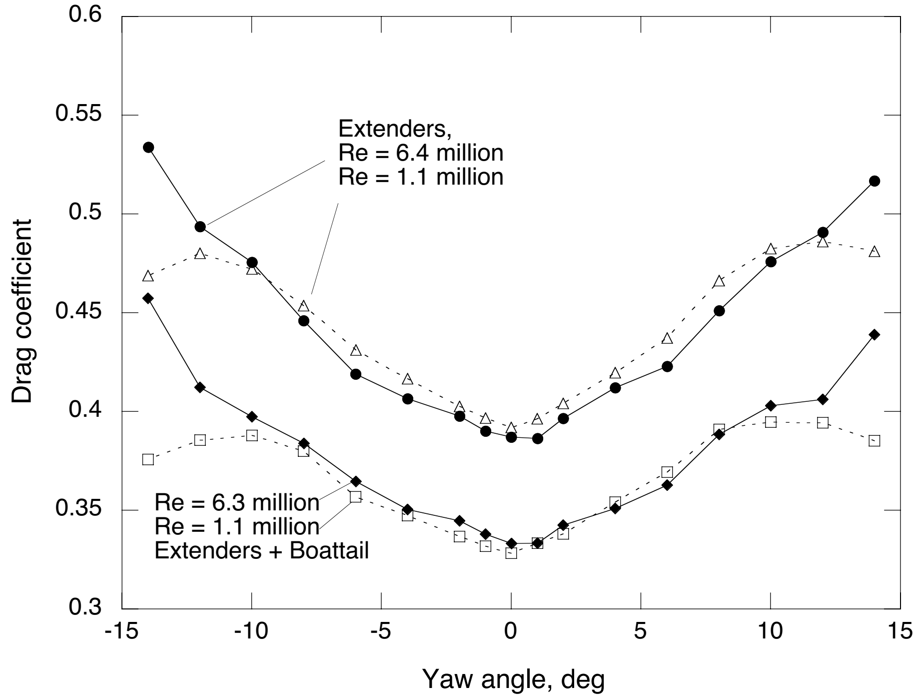

Figure 15: Effect of boattail plates on total drag coefficient.

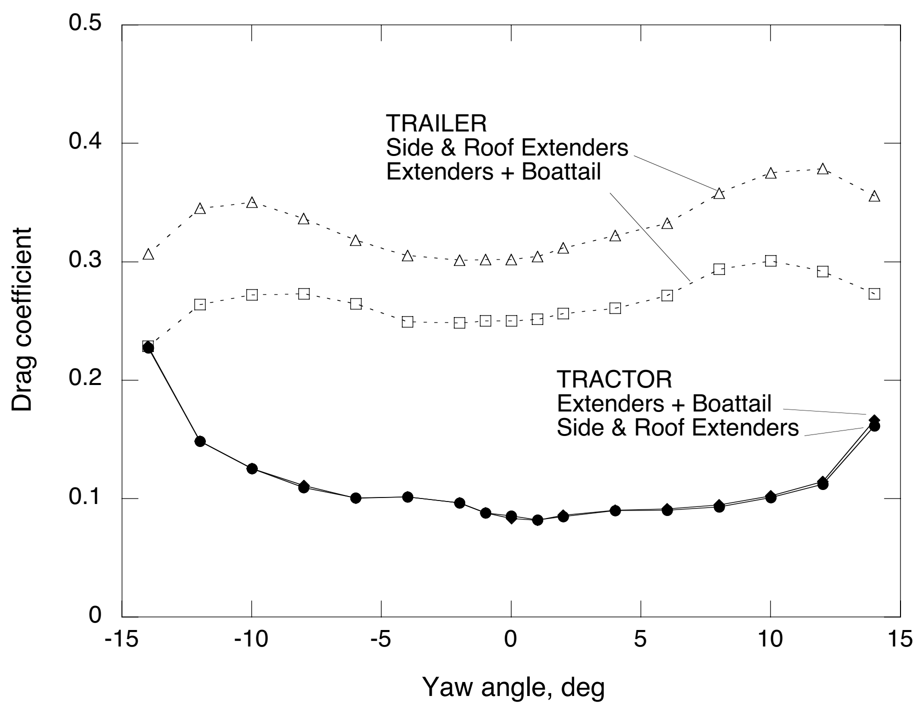

Figure 16: Effect of boattail plates on component drag curves at Re = 6 million.

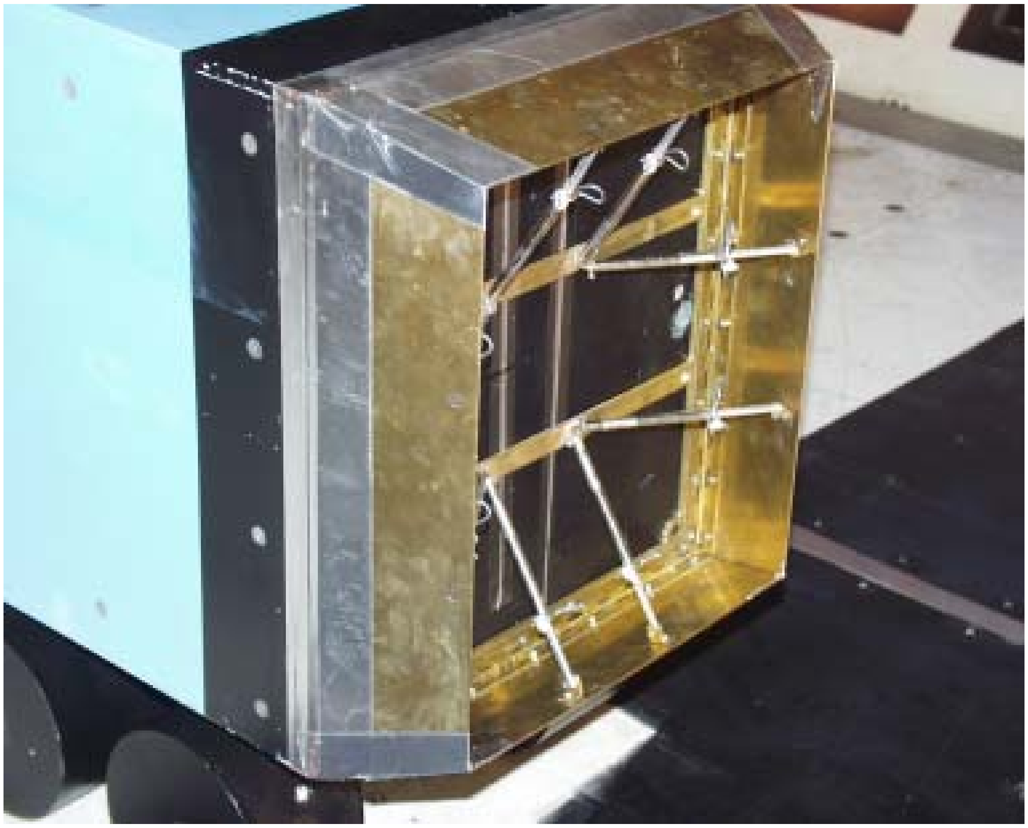

Figure 17: Base flaps installed on trailer base (flap angle = 20 deg).

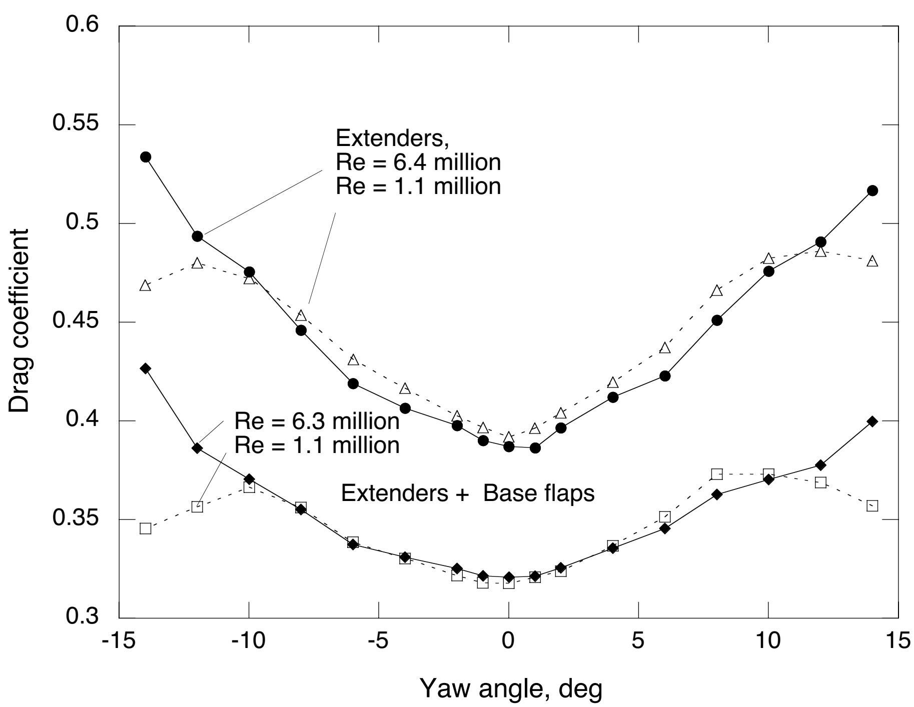

Figure 18: Effect of 16-deg base flaps of total drag coefficient.

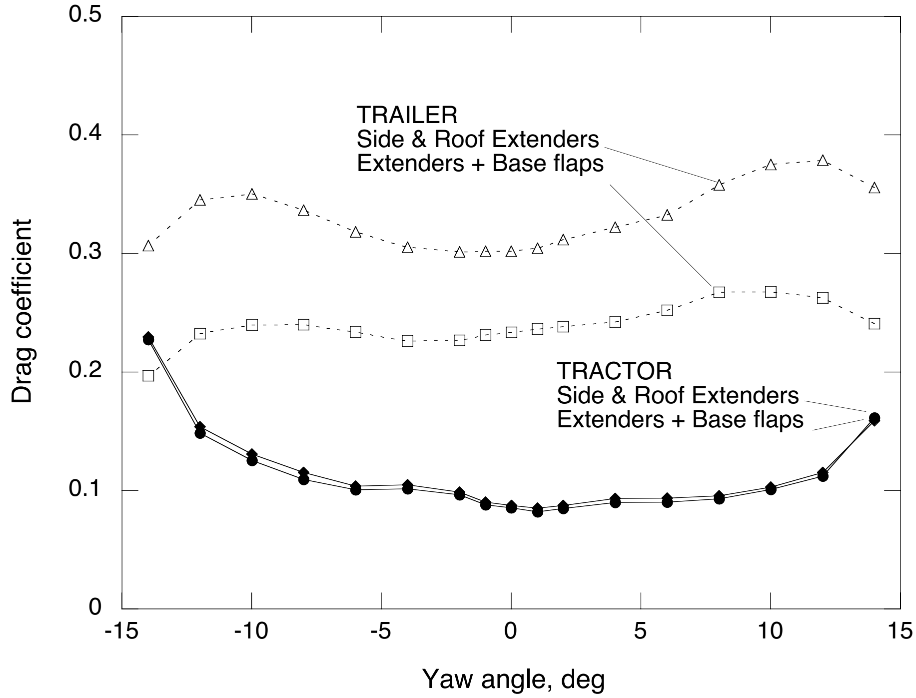

Figure 19: Effect of 16-deg base flaps of component drag curves at Re = 6 million.

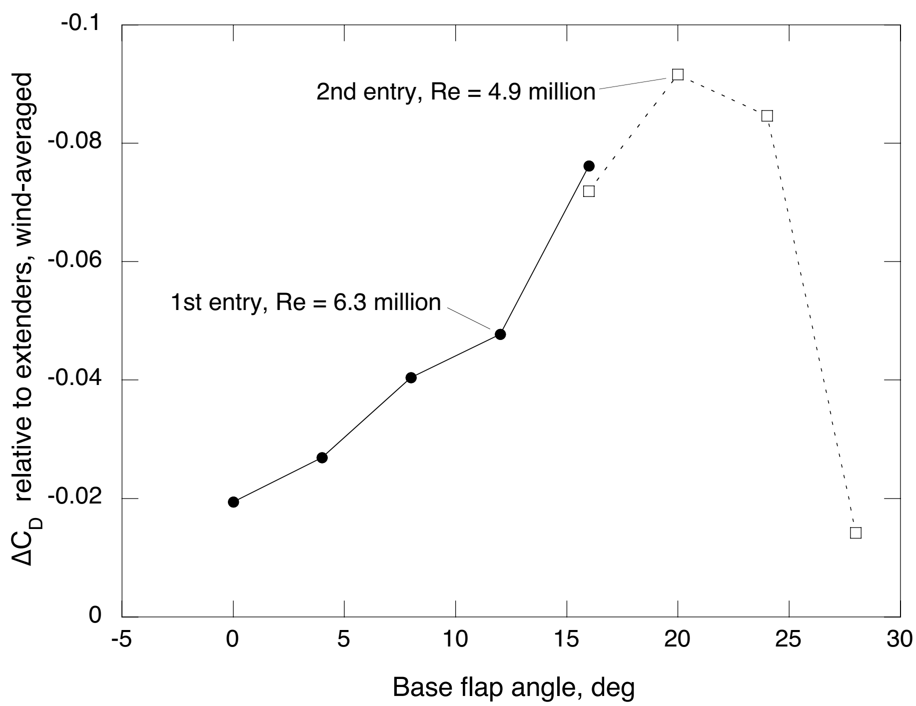

Figure 20: Effect of base-flap angle on wind-averaged drag reduction.

a) Baseline (no belly box)

b) Trailer with belly box

Figure 21: Rear view of trailer with and without belly box.

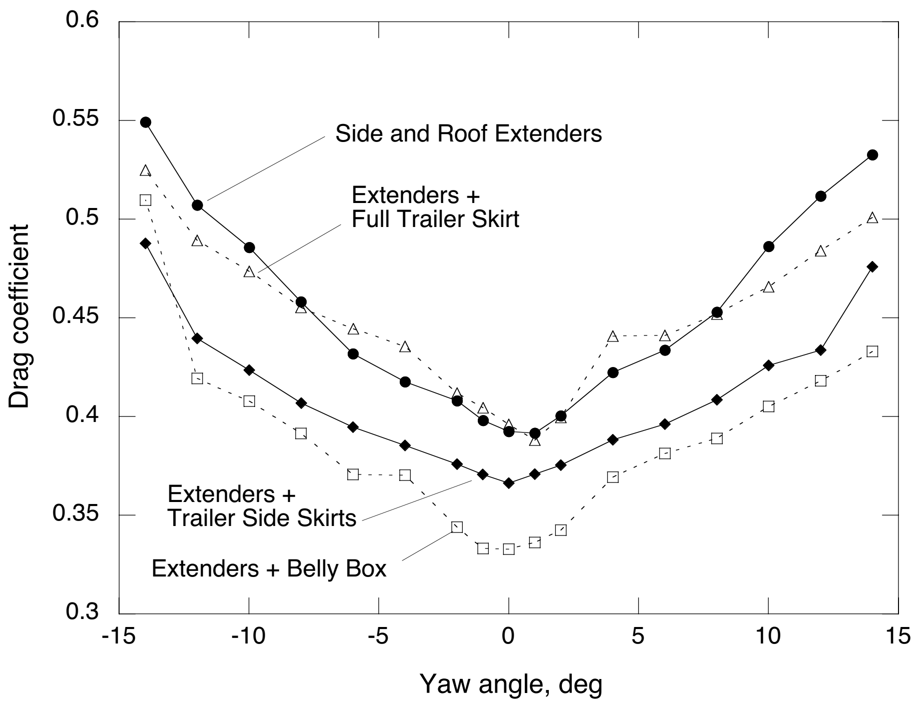

Figure 22: Effect of trailer belly box and skirts on total drag coefficient (Re = 6.3 million).

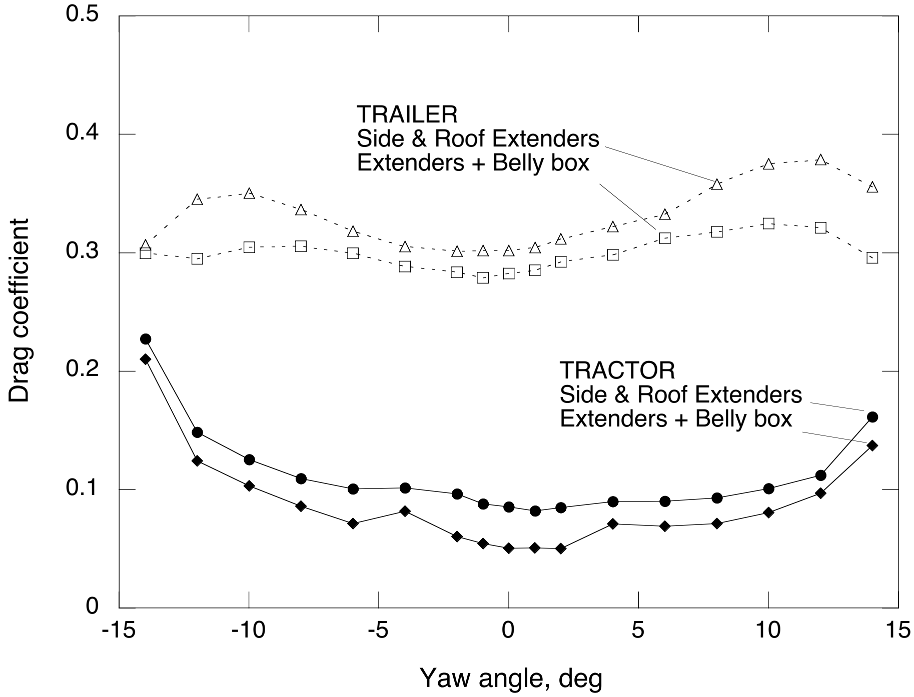

Figure 23: Effect of belly box on component drag curves at Re = 6 million.